Title

Prospects for Employing Lithium Copper Phosphates as High-Voltage Li-Ion Cathodes

Journal

The Journal of Physical Chemistry C, 125(24)

ISSN

1932-7447

Authors

Vincent, Rebecca C
Shen, Jimmy-Xuan
Preefer, Molleigh B
et al.

Publication Date

2021-06-24

DOI

10.1021/acs.jpcc.1c01406

Peer reviewed

Lithium Copper Phosphates as High Energy Density Li-Ion Cathodes

Rebecca C. Vincent,[†,‡] Jimmy-Xuan Shen,[¶,§] Molleigh B. Preefer,[‖,‡] Justin Lin,[‡,⊥] Fabian Seeler,[#] Kerstin Schierle-Arndt,[#] Kristin A. Persson,[*,¶,@] and Ram Seshadri[*,‡,†,‖]

†*Materials Department, University of California Santa Barbara, California 93106, United States*

‡*Materials Research Laboratory, University of California Santa Barbara, California 93106, United States*

¶*Department of Materials Science and Engineering, University of California Berkeley, California 94720, United States*

§*Environmental Energy Technologies Division Lawrence Berkeley National Laboratory Berkeley, California 94720, United States*

‖*Department of Chemistry and Biochemistry, University of California Santa Barbara, California 93106, United States*

⊥*Department of Chemical Engineering, University of California Santa Barbara, California 93106, United States*

#*BASF SE, 67056 Ludwigshafen, Germany*

@*Molecular Foundry, Lawrence Berkeley National Laboratory Berkeley, California 94720, United States*

E-mail: kapersson@lbl.gov; seshadri@mrl.ucsb.edu

Abstract

Three compositions of lithium copper phosphates: Li_2CuPO_4, $Li_2Cu_5(PO_4)_4$, and $Li_2CuP_2O_7$ have been studied as high-voltage cathode materials for Li-ion batteries, following computational predictions of high operating voltages. An assisted-microwave preparation of Li_2CuPO_4, which is otherwise difficult to prepare in nearly-pure form, has been developed. The electrochemical performance of all three compounds has been investigated. The cyclability of these materials is found to be poor due to structural changes, irreversible reduction to metallic copper even at potentials as high as 2.5 V, and the possibility of dissolution into the electrolyte. Some general understanding in regard to the use of Cu compounds in redox electrodes is presented.

Keywords

cathode, lithium-ion battery, lithium copper phosphates, electrochemistry

Introduction

Since the commercialization of lithium-ion batteries (LIBs) in the early 1990s, there has been a continual demand to improve their energy density, which would allow for smaller and lighter portable electronics, and for improved range and performance in electric vehicles. However, the principal chemistry has changed very little since the original LIB; graphite is still employed as the anode, and the most commonly used cathode is a variant of the originally used $LiCoO_2$, notably $Li(Mn, Co, Ni)O_2$ (NMC), with the advantage that the use of toxic and geopolitically fraught Co is partially replaced by Mn and Ni.[1] Depending on the precise composition, NMC has an average operating voltage of about 3.7 V and a gravimetric capacity approaching 200 mAh g^{-1}.[2] New electrode materials, and especially new cathode materials with higher operating voltages and higher capacities are necessary to build cells with increased energy density compared to current technologies.[2,3]

One way to improve the energy density of the cathode is by replacing oxygen anions with polyanions within the crystal structure. For example, phosphates exhibit higher voltages than oxides for the same transition metal redox couples, which can be explained by an inductive effect. Electronegative phosphorous atoms share a common oxygen with the transition metal and attract electrons from the oxygen. Thus, the metal-oxygen bond becomes more ionic, and the voltage of the cathode increases versus lithium.[4]

Olivine-structured transition metal phosphates have been extensively researched as LIB cathode materials. $LiFePO_4$ was proposed as an inexpensive, nontoxic alternative to $LiCoO_2$ in 1997.[5] While initially limited by ionic and electronic conductivity,[6] the performance was significantly improved through nanostructuring and carbon-coating $LiFePO_4$.[7–13] The material has been commercialized, and a capacity of 160 mAh g^{-1} can be accessed at normal rates.[9,10] However, the average operating voltage of $LiFePO_4$ is limited to around 3.45 V by the Fe^{2+}/Fe^{3+} redox couple, which limits the energy density.[5,14]

Mn, Co, and Ni are the three transition metals besides Fe that form olivine structures with PO_4^{3-}. Padhi, Nanjundaswamy, and Goodenough originally reported that they were unable to electrochemically extract lithium from $LiMnPO_4$, $LiCoPO_4$, or $LiNiPO_4$ olivines.[5] Since then, cycling has been demonstrated in $LiCoPO_4$ and $LiMnPO_4$.[15,16] Pure $LiNiPO_4$ has not been experimentally characterized because of difficulties in sample preparation without major impurity phases like $Li_4P_2O_7$ and Ni_3P,[17] and because typical carbonate-based electrolytes are not compatible with the predicted high operating voltage of 5.2 V.[6] $LiCoPO_4$ has a high discharge voltage of 4.8 V, however it contains Co which is expensive, and demonstrates a low capacity of 70 mAh g^{-1}.[15] $LiMnPO_4$ is more promising, demonstrating a practical capacity of 140 mAh g^{-1} and a discharge voltage plateau at 4 V.[16] However, stable cycling was not demonstrated past 50 cycles, and there is still some concern that a Jahn-Teller lattice distortion in Mn^{3+} could lead to capacity fade in longer-term cycling.[16,18]

Combining the most electronegative, redox-active, first-row transition metal and a

phosphate polyanion, lithium copper phosphates appear to be the ideal, high-voltage cathode candidate. However, lithium copper phosphates have been largely untested as cathode materials. Some work has been done to study Li_2CuPO_4, which has a theoretical gravimetric capacity of over 150 mAh g^{-1} when utilizing the Cu^+/Cu^{2+} redox couple.[4,19] As calculated in prior work[4] and shown experimentally,[19] it is difficult to isolate this phase in the Li_3PO_4 - Cu_3PO_4 quasi-binary system. The structure of the desired compound was modeled from single crystal and powder diffraction data, as represented in Figure 1(a) and (b).[19] These initial results suggest a structure with 1D diffusion pathways for lithium ions. (Note: the structure is quite different from an olivine, and Cu is tetrahedrally coordinated, unlike Fe which is octahedrally coordinated in $LiFePO_4$.) Some initial galvanostatic cycling results were obtained between 3 V and 4 V at a rate of $C/30$, and a voltage plateau was observed at a high voltage (about 3.9 V).[19] However, upon further charging, less than one tenth of a lithium ion was extracted per formula unit, and even fewer were reinserted into the structure upon discharge.[19]

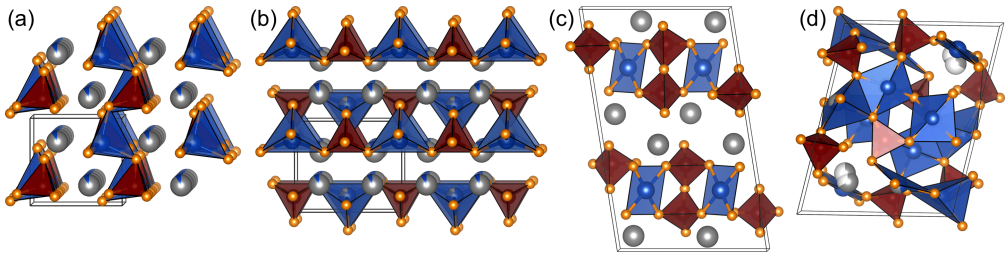

Figure 1: Reported structures of (a) $Li_{2.05}Cu_{0.95}PO_4$ projected nearly down the a-axis and (b) the structure projected nearly down the c-axis.[19] The structures of (c) $Li_2CuP_2O_7$ projected nearly down the b-axis. (d) The structure of $Li_2Cu_5(PO_4)_4$ projected nearly down the a-axis.

Here we study three different compositions of lithium copper phosphates: Li_2CuPO_4, $Li_2CuP_2O_7$, and $Li_2Cu_5(PO_4)_4$. Since the exact cation positions at different degrees of Li insertion are not known *a priori*, we use a general cation insertion algorithm[20] to determine the atomic structure at all stages of charge, which enables us to predict the voltage and capacity of the materials using first-principles calculations. We report a new assisted-microwave preparation of Li_2CuPO_4 and investigate the origins of its poor electrochemical

performance. We also synthesize $Li_2Cu_5(PO_4)_4$ and $Li_2CuP_2O_7$ and investigate their electrochemical properties for the first time.

Experimental methods

Assisted-microwave preparation of Li_2CuPO_4 First, $Li_4P_2O_7$ was prepared by hand grinding a 1:1 molar ratio of Li_2CO_3 (Sigma, $\geq$ 99%) and $NH_4H_2PO_4$ (Sigma, $\geq$ 98%) for 20 min in an agate mortar and pestle. A pellet of the mixture was then placed on a powder bed of the same composition in an alumina crucible, heated to 250 °C for 10 h, then to 800 °C for 4 h and ramped down to room temperature in a box furnace.[21] The powder X-ray diffraction pattern fit of the resulting pure $Li_4P_2O_7$ is provided in the Supporting Information (SI) in Figure S1.

The microwave preparation of Li_2CuPO_4 was adapted from the solid-state furnace methods described in prior work.[19] Cu_2O (Sigma Aldrich, $\geq$ 99.9%) and $Li_4P_2O_7$ were ground with an agate mortar and pestle in a 1:1 stoichiometric ratio until the mixture was homogeneous, about 20 min. The powder was then pressed into a 6 mm diameter pellet, approximately 200 mg. The pellet was sealed into an approximately 10 cm long fused silica ampoule under vacuum. The ampoule was placed at the center of an alumina crucible and buried under 78 g of activated charcoal as described by Levin *et al.*[22] The entire crucible was enclosed by thermal insulation housing made from alumina fiberboard, and the assembly was placed off-center in a 1200 W Panasonic microwave. Many varying microwave procedures were attempted, and the highest purity product was obtained by heating the sample with a power of 720 W for 9 min, at which point the entire alumina fiberboard housing was removed from the microwave. The ampule was extracted and left to cool in air. The temperature of the charcoal was immediately measured at approximately 700 °C by placing a thermocouple in the center of the crucible where the ampoule was. The sample likely reached higher temperatures inside the microwave, however the temperature

cannot be measured continuously during the reaction because a thermocouple in the microwave could result in a fire or explosion. The reddish color of the product is consistent with the desired Cu^{+} oxidation state in the target compound.

Solid-state, furnace synthesis of Li_2CuPO_4, $Li_2CuP_2O_7$, and $Li_2Cu_5(PO_4)_4$ In addition to the microwave method, Li_2CuPO_4 was prepared in a box furnace. Following the initial steps of the microwave preparation, the pelletized mixture was sealed under vacuum into a fused silica ampoule and held at 650 °C for 72 h.

Polycrystalline $Li_2CuP_2O_7$ was synthesized from a ground stoichiometric mixture of Li_2CO_3 (Sigma, $\geq$ 99%), $CuC_2O_4 \cdot 0.5\,H_2O$ (Alfa Aesar 98%), and $(NH_4)_2HPO_4$ (Sigma, $\geq$ 98%) in a molar ratio of 1:1:2 respectively. The powder was heated at 300 °C for three days under Ar gas flow with two intermediate grinding steps. The powder was then pressed into 6 mm pellets and heated at 600 °C for 24 h under Ar gas flow resulting in a light blue product. This method was adapted from a reported procedure that was used to make polycrystalline $Li_2CoP_2O_7$.[23] A prior attempt to repeat a different synthesis method to make $Li_2CuP_2O_7$ resulted in a lower purity product.[24]

Polycrystalline $Li_2Cu_5(PO_4)_4$ was prepared based on a method described in the literature starting from a stoichiometric mixture of Li_2CO_3 (Sigma, $\geq$ 99%), CuO (Aldrich, 99.99%), and $NH_4H_2PO_4$ (Sigma, $\geq$ 98%) ground with an agate mortar and pestle.[25] The powder was placed in a ceramic crucible and heated at 600 °C overnight, reground and heated overnight again at 600 °C, and finally pressed at into 6 mm pellets and heated in the furnace at 800 °C for 48 h. The resultant product showed a blue color, indicative of the desired Cu^{2+} oxidation state.

Microscopy Scanning electron microscopy (SEM) on the pristine and ball milled powders was conducted using an FEI Nova Nano 650 FEG SEM at 5 kV with a spot size of 3.

Electrochemical characterization The electrochemical performance of the three lithium copper phosphates was characterized using Swagelok-type cells assembled in an argon-filled glovebox ($H_2O \leq 0.1$ ppm, $O_2 \leq 0.1$ ppm) using polished Li foil as a combined counter and reference electrode. Active material was ball milled with carbon black (TIMCAL Super P) for 20 min in a 7 cm^3 stainless steel ball mill canister and then hand-ground with polytetrafluoroethylene (PTFE with average particle size of 1 μm from Sigma Aldrich) such that the final electrode composition was 60% active material, 30% carbon black, and 10% PTFE binder. 10 mm diameter thick film electrodes were prepared by pressing pellets from this mixture using a hydrostatic pressure of 1.5 tons. Whatman GF/D glass microfiber filters were used as the separator, and cells were flooded with 1 M $LiPF_6$ in ethylene carbonate and dimethylcarbonate (EC/DMC 50/50 *v/v*, Sigma Aldrich) electrolyte.

Cells were cycled using a BioLogic VMP1 potentiostat predominantly at a slow rate of *C*/60, an exception being the faster cycling that was required during the *operando* X-ray diffraction experiments described below. Rates were calculated for a full charge and discharge defined as one Li exchanged per Cu atom in the cathode. For $Li_2CuP_2O_7$, this would correspond to all the Cu^{2+} ions becoming Cu^{3+} upon charging, and for Li_2CuPO_4 and $Li_2Cu_5(PO_4)_4$ reacting fully between Cu^+ and Cu^{2+} and vice versa.

Operando X-ray diffraction was collected using a custom Swagelok-type cell with a Be window approximately 120 μm thick, which allows X-ray penetration. The active material was ground with SuperP and PTFE (60% active material, 30% SuperP, and 10% PTFE) and pressed into a thin 15 mm pellet which was placed directly onto the Be window. $Li_2CuP_2O_7$ was cycled against Li foil using a BioLogic SP-200 poteniostat at a *C*/10 rate with a Whatman glass fiber separator flooded with 1 M $LiPF_6$ in EC/DMC (Sigma Aldrich). A pattern was collected every 20 minutes during the charge and discharge.

Powder X-ray diffraction Powder X-ray diffraction and *operando* X-ray diffraction data were collected using a laboratory-source Panalytical Empyrean diffractometer with Cu-

Kα radiation in reflection geometry. Rietveld analysis was performed using Topas Academic v6.[26] Patterns were refined against previously experimentally determined structures for Li_2CuPO_4,[19] $Li_2CuP_2O_7$,[24] and $Li_2Cu_5(PO_4)_4$.[25] Crystal structures are depicted using VESTA.[27]

Computational approach First-principles density-functional theory (DFT) calculations were performed using the Vienna *Ab initio* Simulation Package (VASP).[28] The exchange-correlation contribution to the total energy was calculated using the generalized-gradient approximation functional of Perdew-Burke-Ernzerhof (PBE).[29] The determination of the exact simulation settings, the orchestration of the calculations, and the aggregation of the results are carried out using the `atomate` computational framework.[30] The stable Li positions in the crystal structure at all states of charge are determined using a charge-density based cation insertion algorithm.[20] The voltage is given by the change of the total energy of the electrode material with lithium content.[31,32] Using the DFT total energies from our collection of Li inserted structures, the voltage is defined between any two stable lithium concentrations (x_1 and x_2) as:

$$V(x) = -\frac{E(\mathrm{Li}_{x_2}\mathrm{Electrode}) - (\mathrm{Li}_{x_1}\mathrm{Electrode}) - (x_2 - x_1)E(\mathrm{Li})}{(x_2 - x_1)F} \quad \forall x_1 < x < x_2\,, \tag{1}$$

Where $E(\mathrm{Li}_{x_i}\mathrm{Electrode})$ is the DFT total energy of an entry on the convex hull of the subset of materials where the host lattice was not significantly perturbed by the insertion of Li.

Results and discussion

Inspiration to study these particular phosphate compositions came from DFT predictions specifically targeting high-voltage, high-capacity electrode materials. Table 1 gives the predicted average insertion voltage and theoretical gravimetric capacity for $Li_2CuP_2O_7$ and

Li_2CuPO_4. In contrast, it was calculated that five Li ions (corresponding to a Cu^{2+} to Cu^{+} reaction) could not be stably inserted into the $Li_2Cu_5(PO_4)_4$ structure. This likely indicates that the material undergoes a conversion mechanism instead of intercalation.

Table 1: Computational predictions for energy density, average operating voltage, and gravimetric capacity of lithium copper phosphate compounds.

compound	theoretical gravimetric energy density ($Wh\,kg^{-1}$)	predicted average insertion voltage (V)	theoretical gravimetric capacity ($mAh\,g^{-1}$)
$LiCu^{III}P_2O_7$ — $Li_2Cu^{II}P_2O_7$	490	4.60	107
$LiCu^{II}PO_4$ — $Li_2Cu^{I}PO_4$	606	3.90	156
$Li_2Cu^{II}_5(PO_4)_4$ — $Li_7Cu^{I}_5(PO_4)_4$	N/A	N/A	188

$Li_2CuP_2O_7$

The structure of $Li_2CuP_2O_7$ is shown in Figure 1(c), exhibiting an open structure with tunnel-like cavities.[24] This is the first demonstration of synthesizing $Li_2CuP_2O_7$ via solid-state methods using copper oxalate, lithium carbonate, and diammonium phosphate as precursors (see Figure 2(a) for the powder X-ray diffraction pattern fit). Using this method resulted in sub-micron to 10 micron diameter particles as shown in Figure 2(b). $Li_2CuP_2O_7$ is an electronically-insulating material (light blue in color), so the material was ball milled with carbon black prior to electrochemical testing (see Figure 2(c)).

During initial galvanostatic cycling, as shown in Figure 3(a), $Li_2CuP_2O_7$ was charged to 4.8 V and then discharged to 1 V at a very slow rate of *C*/60, resulting in a long discharge plateau between 1.75 V and 1.6 V. This plateau likely corresponds to a conversion reaction during which the copper is reduced to its metallic form as more lithium is incorporated into the cathode. Subsequent cycling failed, indicating that the low voltage reaction is irreversible. Figure 3(b) shows cycling between 4.8 V and 1.7 V at a rate of *C*/60. A high-voltage oxidation plateau is present at the predicted voltage of 4.6 V (as given in Table 1). The detrimental low voltage plateau was not totally eliminated, so the lower potential

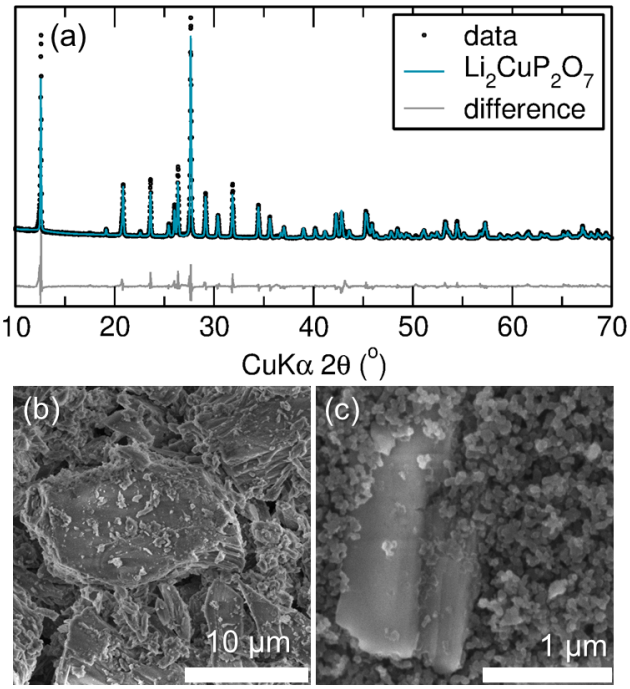

Figure 2: (a) Rietveld refinement fit of the powder X-ray diffraction pattern of the $Li_2CuP_2O_7$ synthesized via solid-state methods. (b) Scanning electron micrograph of as-synthesized $Li_2CuP_2O_7$ particles ranging in size from sub-micron to 10 microns in diameter. (c) Scanning electron micrograph of $Li_2CuP_2O_7$ after ball milling with carbon black prior to electrochemical testing. Ball milled particles range in size from sub-micron to 1 micron in diameter.

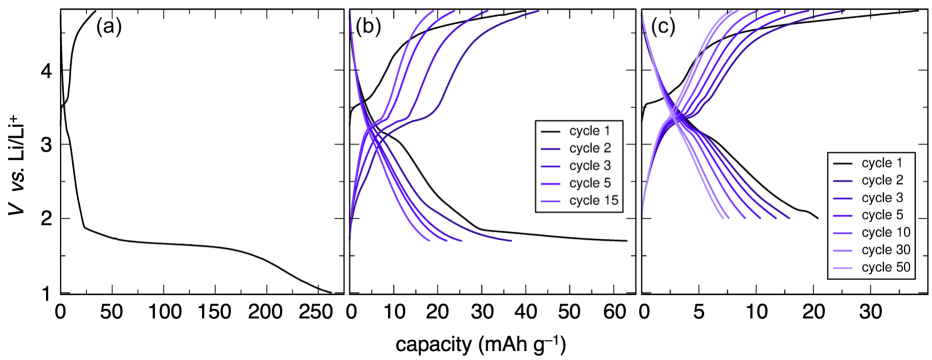

Figure 3: (a) Galvanostatic cycling of ball milled $Li_2CuP_2O_7$ between and 4.8 V and 1 V at a $C/60$ rate, (b) between 4.8 V and 1.7 V at a $C/60$ rate, and (c) between 4.8 V and 2 V at a $C/30$ rate.

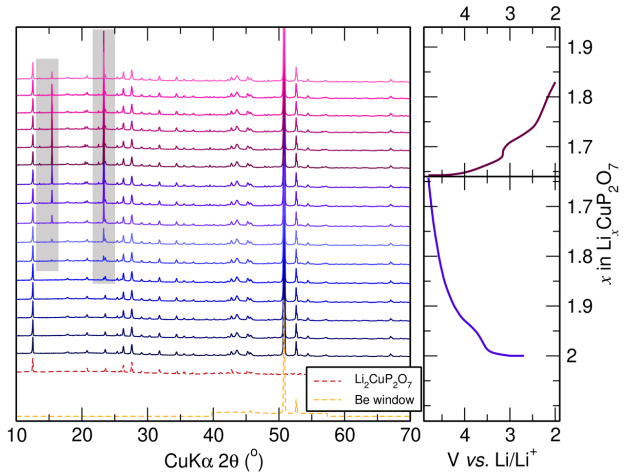

Figure 4: *Operando* X-ray diffraction measured every 20 min during a galvanostatic charge to 4.8 V and discharge to 2 V of ball milled $Li_2CuP_2O_7$ at a $C/10$ rate. Below the incremental XRD scans, which peaks correspond to the $Li_2CuP_2O_7$ active material and which peaks correspond to the beryllium window of the operando cell are displayed. The most obvious changes during cycling are shaded.

was further limited to 2 V as shown in Figure 3(c). Figure 4 shows XRD spectra measured every 20 minutes during a charge and discharge cycle of $Li_2CuP_2O_7$. Upon charging, two new XRD peaks emerge, one near 15 degrees and the other near 25 degrees. These peaks diminish but do not disappear completely upon discharge, indicating structural irreversibility. A heat map highlighting the changes in X-ray diffraction pattern peak intensity during cycling is provided in the SI (Figure S2). $Li_2CuP_2O_7$ did not achieve a meaningful reversible capacity during any of the cycling experiments. By charging first, Li is removed from $Li_2CuP_2O_7$ corresponding to Cu^{2+} becoming Cu^{3+}, an oxidation state of Cu which is difficult to reach through electrochemical cycling. Cu^{3+} containing compounds are rare, and often require very oxidizing conditions during preparation.[33,34]

Li_2CuPO_4

The approximate structure of Li_2CuPO_4 is given in Figure 1(a) and (b).[19] Motivation for using microwave preparation arose from the reported difficulty of isolating different stable phases in a furnace.[19] The highest purity, 90%, was achieved with 9 min of microwave

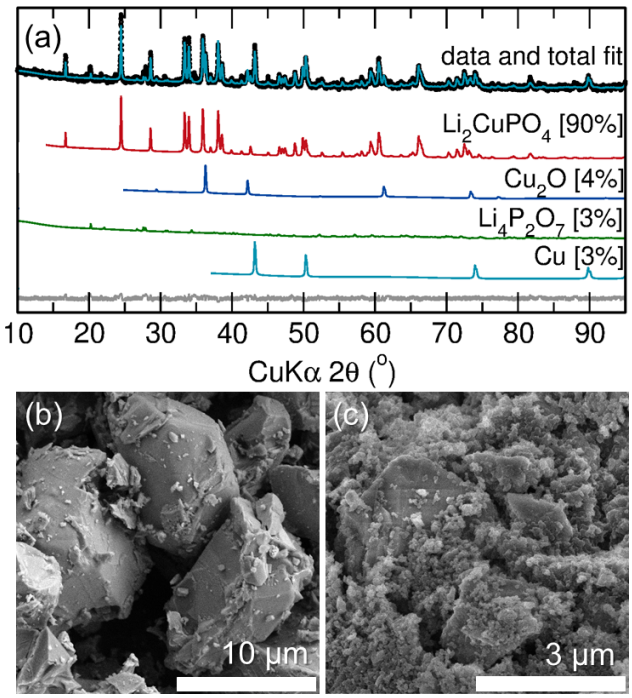

Figure 5: (a) Rietveld refinement of microwave-prepared Li_2CuPO_4. (b) Scanning electron micrograph of assisted-microwave-prepared Li_2CuPO_4 particles ranging in size from sub-micron to 10 μm in diameter, and (c) the same particles after ball milling with carbon black prior to electrochemical testing. Ball milled particles range in size from sub-micron to 3 μm in diameter.

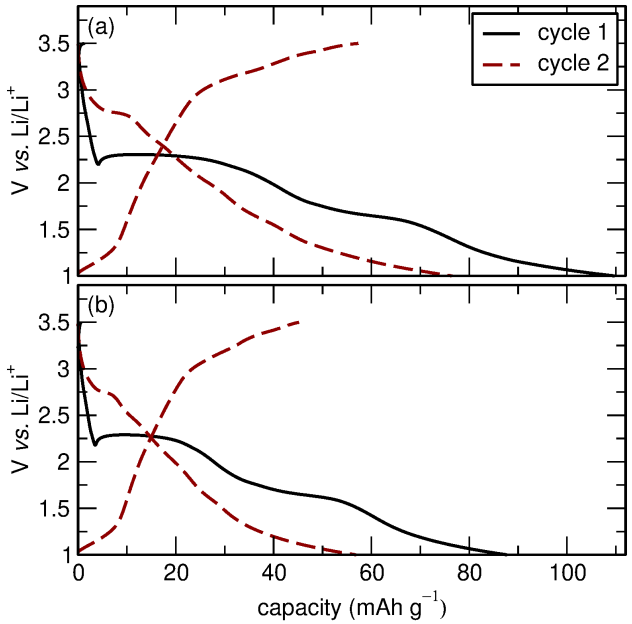

Figure 6: Galvanostatic cycling of (a) ball milled, microwave-prepared Li_2CuPO_4 at a rate of $C/60$ and (b) ball milled, furnace-prepared Li_2CuPO_4 at a rate of $C/60$.

heating at 720 W, and the Rietveld refinement is shown in Figure 5(a). SEM images of the microwave product before and after ball milling with carbon black are given in Figure 5(b) and (c). Before milling, the particles range in diameter from sub-micron to 10 μm, and after ball milling with carbon black the particles range in size from sub-micron to 3 μm in diameter. The most successful furnace synthesis attempt yielded 73% purity, with 17% of the sample identified as a related phase with higher lithium content, $Li_{2.6}Cu_{0.4}PO_4$.[19] The Rietveld refinement fit of the furnace product is given in the SI (Figure S3), along with SEM images before and after ball milling with carbon black.

Figure 6 compares galvanostatic cycling behavior of the microwave-prepared Li_2CuPO_4 to the furnace-prepared Li_2CuPO_4. Differences in capacity achieved by these cells can be explained by the difference in purity of the active material that was achieved with the microwave versus in the furnace. Li_2CuPO_4 could not be cycled above a potential of 3.5 V: cells regularly failed to charge above this potential. Thus, the computationally predicted average voltage of 3.9 V (given in Table 1) could not be reached. Cell failure occurs when a build up of internal resistance causes the potentiostat to stop charging the cell. Failure above a potential of 3.5 V could be due to a side reaction forming a resistive electrode-electrolyte interface layer, or breakdown at the surface of the cathode material, such as Cu dissolution into the organic electrolyte in the form of Cu^+ which has been shown to occur in this same voltage range.[35–37]

$Li_2Cu_5(PO_4)_4$

$Li_2Cu_5(PO_4)_4$ is a known material that is closest in composition to delithiated Li_2CuPO_4. $LiCuPO_4$ has never been directly synthesized, however the composition of $Li_2Cu_5(PO_4)_4$ is close, and still has Cu in a 2+ oxidation state. The structure of $Li_2Cu_5(PO_4)_4$ is shown in Figure 1(d), and a Rietveld refinement fit of the solid-state synthesized polycrystalline material is shown in Figure 7(a). SEM images of the particles before and after ball milling with carbon black are given in Figure 7(b) and (c), and show as-synthesized $Li_2Cu_5(PO_4)_4$

particles ranging in size from 5 μm to almost 50 μm in diameter. After ball milling with carbon black, particles range in size from sub-micron to 5 μm in diameter.

Galvanostatic cycling of $Li_2Cu_5(PO_4)_4$ is shown in Figure 8. The first discharge shown in Figure 8(a) exhibits an impressive gravimetric capacity of over 300 mAh g^{-1}. However, capacity fades significantly on subsequent cycles. 300 mAh g^{-1} exceeds the theoretical capacity of 188 mAh g^{-1} calculated for single electron redox, so it is probable that Cu^{2+} is being reduced to metallic copper at around 2.25 V. A conversion reaction is consistent with our computational prediction that Li would not intercalate into the $Li_2Cu_5(PO_4)_4$ structure. When discharging CuF_2, a one-step lithiation reaction forming Cu^0 and LiF occurs at a potential as high as 3.25 V, which further supports that metallic Cu could be forming at 2.25 V in $Li_2Cu_5(PO_4)_4$.[35,38] The additional capacity could also be due to side reactions or degradation of the electrolyte.

The voltage profile of $Li_2Cu_5(PO_4)_4$ is similar to that of Li_2CuPO_4, which makes sense due to their similar compositions. They both show a local voltage minimum around 2.25 V, at least in the first discharge, which could correspond to the nucleation of metallic copper.

Conclusions

Three compositions of lithium copper phosphate: $Li_2CuP_2O_7$, Li_2CuPO_4, and $Li_2Cu_5(PO_4)_4$ were evaluated as high-voltage cathode materials for Li-ion batteries. An assisted-microwave preparation of Li_2CuPO_4 was developed, as well as a solid-state, furnace synthesis for $Li_2CuP_2O_7$ using copper oxalate as a precursor. $Li_2Cu_5(PO_4)_4$ and $Li_2CuP_2O_7$ were electrochemically cycled for the first time. A few complications prevented useful electrochemical cycling of these materials. Li could not be significantly deintercalated from $Li_2CuP_2O_7$ likely because an oxidation state of Cu^{3+} could not be stabilized in the structure. Discharging to lower voltages and attempting to insert more Li resulted in an irreversible conversion reaction below 2 V. Li_2CuPO_4 could not be cycled much higher than 3.5 V, above

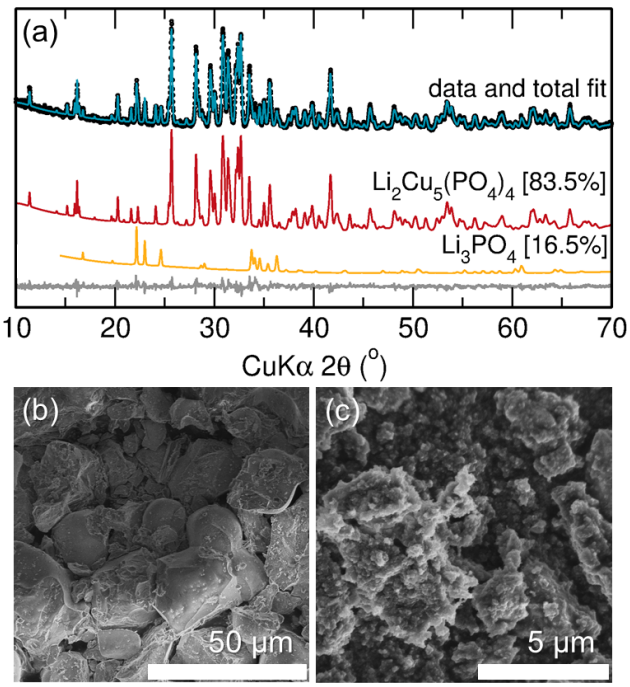

Figure 7: (a) Rietveld refinement fit of the powder X-ray diffraction pattern of the $Li_2Cu_5(PO_4)_4$ (b) Scanning electron micrograph of as-synthesized $Li_2Cu_5(PO_4)_4$ particles ranging in size from 5 μm to almost 50 μm in diameter. (c) Scanning electron micrograph of $Li_2Cu_5(PO_4)_4$ after ball milling with carbon black and prior to electrochemical testing. Particles range in size from sub-micron to 5 μm in diameter.

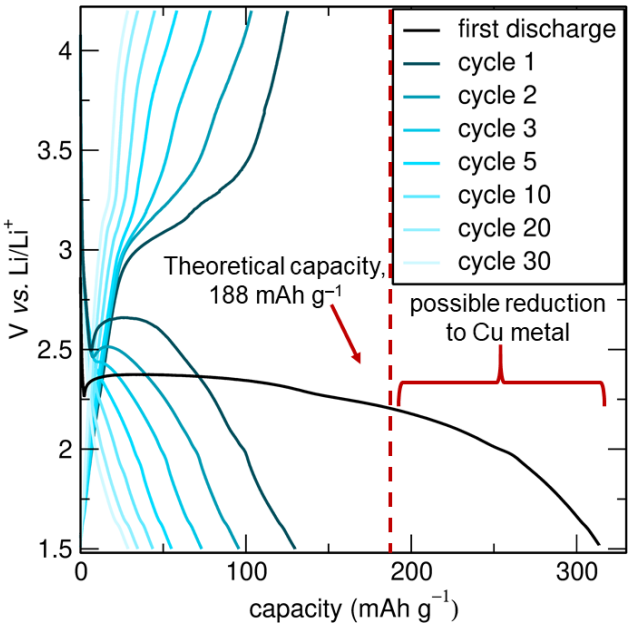

Figure 8: (a) Galvanostatic cycling of ball milled $Li_2Cu_5(PO_4)_4$ at a $C/60$ rate between 1.5 V and 4.2 V.

which more significant redox activity was expected. In the literature reported cycling of CuF_2, much of the irreversibility was attributed to the dissolution of Cu^+ into organic electrolyte.[35] $Li_2Cu_5(PO_4)_4$ was then prepared as the closest known composition to that of delithiated Li_2CuPO_4. Upon initial discharge, a very large capacity of over 300 mAh g^{-1} was observed. However, because the observed capacity was significantly greater than the theoretical capacity of 188 mAh g^{-1}, it is likely that much of the observed capacity is due to reduction of the Cu^{2+} to metallic copper at a potential of 2.5 V. Reduction to metallic copper would also explain the continued capacity fade observed on subsequent cycling. A conversion reaction of this nature is consistent with the computational prediction that Li intercalation is unlikely in the $Li_2Cu_5(PO_4)_4$ structure.

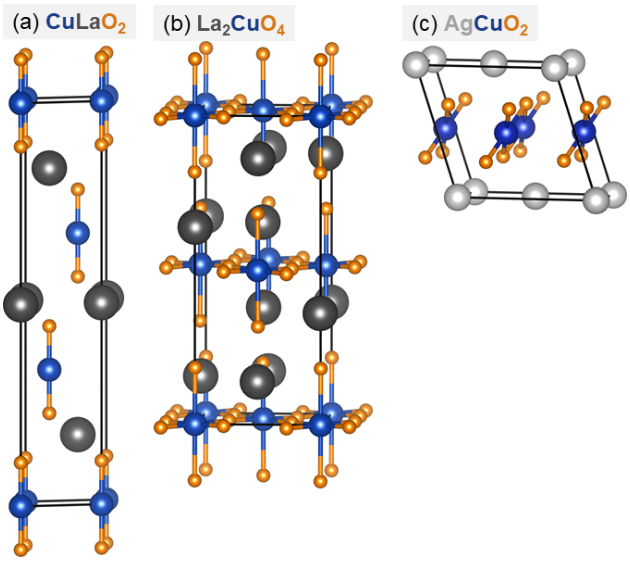

Figure 9: (a) The crystal structure of $CuLaO_2$, in which Cu^+ has linear coordination.[39] (b) The crystal structure of La_2CuO_4, in which Cu^{2+} sits in highly Jahn-Teller distorted octahedra.[40] (c) The crystal structure of $AgCuO_2$, in which Cu^{3+} has square planar coordination.[33]

Another important challenge with utilizing copper redox in an intercalation compound (as opposed to a conversion compound) is that the different oxidation states of Cu favor different coordination. Cu^+ has a d^{10} electron configuration and prefers tetrahedral coordination [Figure 1(a) and (b)] or linear coordination [Figure 9(a)], while Cu^{2+} is d^9 and prefers square planar [Figure 1(c) and (d)], or highly Jahn-Teller distorted octahe-

dral coordination [Figure 9(b)]. Cu^{3+} is d^8 and also prefers square planar coordination [Figure 9(c)]. The different coordination preferences can contribute to structural degradation and irreversible cycling, as shown for Li_2CuPO_4 and $Li_2Cu_5(PO_4)_4$ in Figures 6 and 8 respectively. Similar degradation mechanisms have been shown to contribute to the irreversibility of redox compounds containing Mn^{3+}, most notably $LiMn_2O_4$ spinels.[41,42]

Supporting Information Available

Rietveld refinement fit of the powder X-ray diffraction pattern of $Li_4P_2O_7$, a precursor prepared *via* solid-state methods for the reaction to form Li_2CuPO_4. Rietveld refinement and microscopy of the furnace prepared Li_2CuPO_4. Heat map of $Li_2CuP_2O_7$ operando XRD measured during galvanostatic cycling.

Acknowledgement

This work was supported by BASF Corporation through the California Research Alliance. The research reported here made use of shared facilities of the National Science Foundation (NSF) Materials Research Science and Engineering Center (MRSEC) at UC Santa Barbara, NSF DMR 1720256, a member of the Materials Research Facilities Network (www.mrfn.org). The computational infrastructure work gratefully acknowledges the US Department of Energy, Office of Science, Office of BasicvEnergy Sciences, Materials Sciences and Engineering Division under contract no. DE-AC02-05-CH11231 (Materials Project program KC23MP). **RCV acknowldeges the NSF for a Graduate Research Fellowship, grant number 1650114.**

References

(1) Blomgren, G. The Development and Future of Lithium Ion Batteries. *J. Electrochem. Soc.* **2017**, *164*, A5019–25.

(2) Hayner, C. M.; Zhao, X.; Kung, H. H. Materials for Rechargeable Lithium-ion Batteries. *Annu. Rev. Chem. Biomol. Eng.* **2012**, *3*, 445–71.

(3) Goodenough, J. B.; Park, K. S. The Li-Ion Rechargeable Battery: A Perspective. *J. Am. Chem. Soc.* **2013**, *135*, 1167–1176.

(4) Hautier, G.; Jain, A.; Ong, S. P.; Kang, B.; Moore, C.; Doe, R.; Ceder, G. Phosphates as Lithium-ion Battery Cathodes: An Evaluation Based on High-Throughput *ab initio* Calculations. *Chem. Mater.* **2011**, *23*, 3495–3508.

(5) Padhi, A. K.; Nanjundaswamy, K. S.; Goodenough, J. B. Phospho-Olivines as Positive-Electrode Materials for Rechargeable Lithium Batteries. *J. Electrochem. Soc.* **1997**, *144*, 1188–94.

(6) Morgan, D.; Van der Ven, A.; Ceder, G. Li Conductivity in Li_xMPO_4 (M = Mn, Fe, Co, Ni) Olivine Materials. *Electrochem. Solid-State Lett.* **2004**, *7*, A30–32.

(7) Wang, Y.; He, P.; Zhou, H. Olivine $LiFePO_4$: Development and Future. *Energy Environ. Sci.* **2011**, *4*, 805–17.

(8) Manthiram, A. Phospho-Olivine Cathodes for Lithium-ion Batteries. *Electrochem. Soc. Interface* **2009**, *18*, 44–47.

(9) Yamada, A.; Chung, S. C.; Hinokuma, K. Optimized $LiFePO_4$ for Lithium Battery Cathodes. *J. Electrochem. Soc.* **2001**, *148*, A224–29.

(10) Huang, H.; Yin, S.-C.; Nazer, L. F. Approaching Theoretical Capacity of $LiFePO_4$ at Room Temperature at High Rates. *Electrochem. Solid-State Lett.* **2001**, *4*, A170–72.

(11) Chueh, W. C.; El Gabaly, F.; Sugar, J. D.; Bartelt, N. C.; McDaniel, A. H.; Fenton, K. R.; Zavadil, K. R.; Tyliszczak, T.; Lai, W.; McCarty, K. F. Intercalation Pathway in Many-particle $LiFePO_4$ Electrode Revealed by Nanoscale State-of-charge Mapping. *Nano Lett.* **2013**, *13*, 866–872.

(12) Jaiswal, A.; Horne, C.; Chang, O.; Zhang, W.; Kong, W.; Wang, E.; Chern, T.; Doeff, M. Nanoscale $LiFePO_4$ and $Li_4Ti_5O_{12}$ for High Rate Li-Ion Batteries. *J. Electrochem. Soc.* **2009**, *156*, A1041.

(13) Li, Y.; Meyer, S.; Lim, J.; Lee, S. C.; Gent, W. E.; Marchesini, S.; Krishnan, H.; Tyliszczak, T.; Shapiro, D.; Kilcoyne, A. L. D., et al. Effects of Particle Size, Electronic Connectivity, and Incoherent Nanoscale Domains on the Sequence of Lithiation in $LiFePO_4$ Porous Electrodes. *Adv. Mater.* **2015**, *27*, 6591–6597.

(14) Goodenough, J. B.; Kim, Y. Challenges for Rechargeable Li Batteries. *Chem. Mater.* **2010**, *22*, 578–603.

(15) Amine, K.; Yasuda, H.; Yamachi, M. Olivine $LiCoPO_4$ as 4.8 V Electrode Material for Lithium Batteries. *Electrochem. Solid-State Lett.* **2000**, *3*, 178–79.

(16) Li, G.; Azuma, H.; Tohda, M. $LiMnPO_4$ as the Cathode for Lithium Batteries. *Electrochem. Solid-State Lett.* **2002**, *5*, A135–37.

(17) Li, W.; Song, B.; Manthiram, A. High-voltage Positive Electrode Materials for Lithium-Ion Batteries. *Chem. Soc. Rev.* **2017**, *46*, 3006–59.

(18) Choi, D.; Wang, D.; Bae, I.-T.; Xiao, J.; Nie, Z.; Wang, W.; Viswanathan, V. V.; Lee, Y. J.; Zhang, J.-G.; Graff, G. L.; Yang, Z.; Liu, J. $LiMnPO_4$ Nanoplate Grown via Solid-State Reaction in Molten Hydrocarbon for Li-Ion Battery Cathode. *Nano Lett.* **2010**, *10*, 2799–2805.

(19) Snyder, K.; Raguz, B.; Hoffbauer, W.; Glaum, R.; Ehrenberg, H.; Herklotz, M. Lithium Copper(I) Orthophosphates $Li_{3-x}Cu_xPO_4$: Synthesis, Crystal Structures, and Electrochemical Properties. *Z. Anorg. Allg. Chem.* **2014**, *640*, 944–51.

(20) Shen, J.-X.; Horton, M.; Persson, K. A. A Charge-Density-Based General Cation Insertion Algorithm for Generating New Li-Ion Cathode Materials. *npj Comput. Mater.* **2020**, *6*, 1–7.

(21) Voronin, V. I.; Sherstobitova, E. A.; Blatov, V. A.; Shekhtman, G. S. Lithium-Cation Conductivity and Crystal Structure of Lithium Diphosphate. *J. Solid State Chem.* **2014**, *211*, 170–75.

(22) Levin, E. E.; Grebenkemper, J. H.; Pollock, T. M.; Seshadri, R. Protocols for High Temperature Assisted-Microwave Preparation of Inorganic Compounds. *Chem. Mater.* **2019**, *31*, 7151–59.

(23) Kim, H.; Lee, S.; Park, Y.-U.; Kim, H.; Kim, J.; Jeon, S.; Kang, K. Neutron and X-ray Diffraction Study of Pyrophosphate-Based $Li_{2-x}MP_2O_7$ (M = Fe, Co) for Lithium Rechargeable Battery Electrodes. *Chem. Mater.* **2011**, *23*, 3930–3937.

(24) Spirlet, M. R.; Rebizant, J.; Liegeois-Duyckaerts, M. Structure of Lithium Copper Pyrophosphate. *Acta Cryst.* **1993**, *C49*, 209–211.

(25) Cui, L.; Pan, S.; Han, J.; Dong, X.; Zhou, Z. Synthesis, Crystal Structure and Optical Properties of $Li_2Cu_5(PO_4)_4$. *Solid State Sci.* **2011**, *13*, 1308–04.

(26) Coelho, A. A. TOPAS and TOPAS-Academic: an Optimization Program Integrating Computer Algebra and Crystallographic Objects Written in C++. *J. Appl. Crystallogr.* **2018**, *51*, 210–218.

(27) Momma, K.; Izumi, F. VESTA: a Three-dimensional Visualization System for Electronic and Structural Analysis. *J. Appl. Crystallogr.* **2008**, *41*, 653–658.

(28) Kresse, G.; Furthmüller, J. Efficiency of Ab-initio Total Energy Calculations for Metals and Semiconductors Using a Plane-wave Basis Set. *Comput. Mater. Sci.* **1996**, *6*, 15–50.

(29) Perdew, J. P.; Burke, K.; Ernzerhof, M. Generalized Gradient Approximation Made Simple. *Phys. Rev. Lett.* **1996**, *77*, 3865.

(30) Mathew, K. et al. Atomate: A High-level Interface to Generate, Execute, and Analyze Computational Materials Science Workflows. *Comput. Mater. Sci.* **2017**, *139*, 140–152.

(31) Van der Ven, A.; Aydinol, M. K.; Ceder, G.; Kresse, G.; Hafner, J. First-Principles Investigation of Phase Stability in Li_xCoO_2. *Phys. Rev. B* **1998**, *58*, 2975–2987.

(32) Urban, A.; Seo, D.-H.; Ceder, G. Computational Understanding of Li-Ion Batteries. *npj Comput. Mater.* **2016**, *2*, 16002.

(33) Curda, J.; Klein, W.; Jansen, M. $AgCuO_2$ – Synthesis, Crystal Structure, and Structural Relationships with CuO and $Ag^{I}Ag^{III}O_2$. *J. Solid State Chem.* **2001**, *162*, 220–224.

(34) Choy, J.-H.; Jung, D.-Y.; Kim, S.-J.; Choi, Q. W.; Demazeau, G. Physicochemical Distinction Between Cu^{3+} and O_2^{2-} in $YBa_2Cu_3O_{6.5+\delta}$ Lattice Upon Oxidation Reaction of Bremide and Spectroscopic Analyses. *Physica C* **1991**, *185–189*, 763–764.

(35) Hua, X.; Robert, R.; Du, L.-S.; Wiaderek, K. M.; Leskes, M.; Chapman, K. W.; Chupas, P. J.; Grey, C. P. Comprehensive Study of the CuF_2 Conversion Reaction Mechanism in a Lithium Ion Battery. *J. Phys. Chem. C* **2014**, *118*, 15169–15184.

(36) Whitehead, A. H.; Schreiber, M. Current Collectors for Positive Electrodes of Lithium-Based Batteries. *J. Electrochem. Soc.* **2005**, *152*, A2105–A2113.

(37) Kawakita, J.; Kobayashi, K. Anodic Polarization Behavior of Copper in Propylene Carbonate. *J. Power Sources* **2001**, *101*, 47–52.

(38) Omenya, F.; Zagarella, N. J.; Rana, J.; Zhang, H.; Siu, C.; Zhou, H.; Wen, B.; Chernova, N. A.; Piper, L. F. J.; Zhou, G.; Whittingham, M. S. Intrinsic Challenges to the Electrochemical Reversibility of the High Energy Density Copper(II) Fluoride Cathode Material. *ACS Appl. Energy Mater.* **2019**, *2*, 5243–5253.

(39) Haas, H.; Kordes, E. Cu^{1+}–Haltige Doppeloxide mit Seltenen Erdmetallen 1. *Z. Kristallographie* **1969**, *129*, 259–270.

(40) Delgado, J.; McMullan, R.; de Delgado, G. D.; Wuensch, B.; Picone, P.; Jenssen, H.; Gabbe, D. Single–Crystal Neutron–Diffraction Study of $La_2Cu_{0.95}Li_{0.05}O_4$. *Phys. Rev. B* **1988**, *37*, 9343.

(41) Rodríguez-Carvajal, J.; Rousse, G.; Masquelier, C.; Hervieu, M. Electronic Crystallization in a Lithium Battery Material: Columnar Ordering of Electrons and Holes in the Spinel $LiMn_2O_4$. *Phys. Rev. Lett.* **1998**, *81*, 4660–4663.

(42) Nakayama, M.; Nogami, M. A First-Principles Study on Phase Transition Induced by Charge Ordering of Mn^{3+}/Mn^{4+} in Spinel $LiMn_2O_4$. *Solid State Commun.* **2010**, *150*, 1329–1333.

Graphical TOC Entry

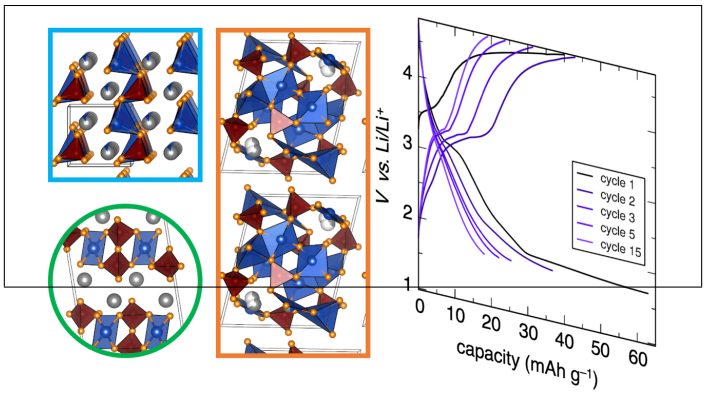

Supporting Information: Prospects for Employing Lithium Copper Phosphates as High-Voltage Li-Ion Cathodes

Rebecca C. Vincent,[†,‡] Jimmy-Xuan Shen,[¶,§] Molleigh B. Preefer,[‖,‡] Justin Lin,[‡,⊥] Fabian Seeler,[#] Kerstin Schierle-Arndt,[#] Kristin A. Persson,[*,¶,@] and Ram Seshadri[*,‡,†,‖]

†*Materials Department, University of California Santa Barbara, California 93106, United States*

‡*Materials Research Laboratory, University of California Santa Barbara, California 93106, United States*

¶*Department of Materials Science and Engineering, University of California Berkeley, California 94720, United States*

§*Environmental Energy Technologies Division Lawrence Berkeley National Laboratory Berkeley, California 94720, United States*

‖*Department of Chemistry and Biochemistry, University of California Santa Barbara, California 93106, United States*

⊥*Department of Chemical Engineering, University of California Santa Barbara, California 93106, United States*

#*BASF SE, 67056 Ludwigshafen, Germany*

@*Molecular Foundry, Lawrence Berkeley National Laboratory Berkeley, California 94720, United States*

E-mail: kapersson@lbl.gov; seshadri@mrl.ucsb.edu

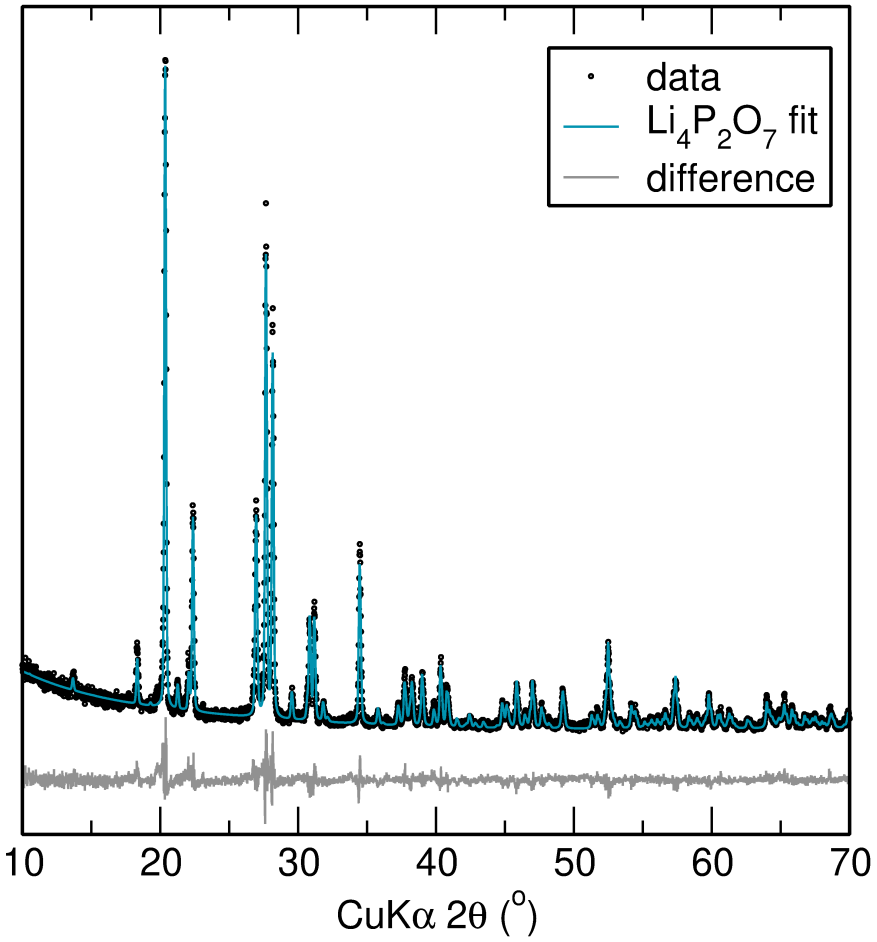

Figure S1: Rietveld refinement of the powder X-ray diffraction pattern of the $Li_4P_2O_7$ synthesized via solid state methods, precursor to Li_2CuPO_4.

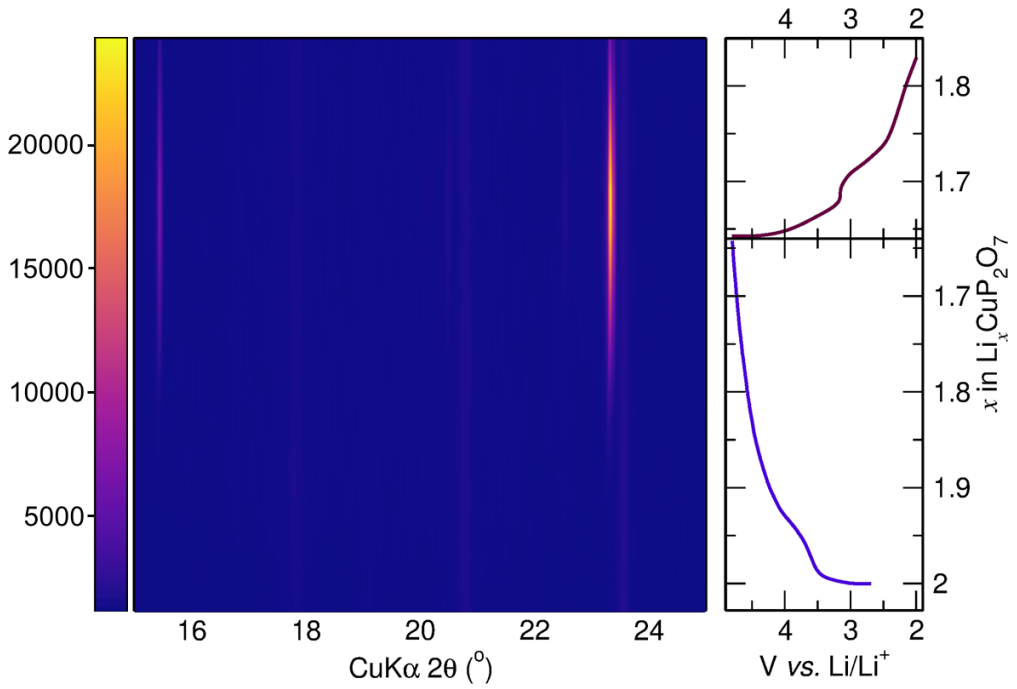

Figure S2: Heat map of the intensity of diffraction peaks during *operando* X-ray diffraction experiment. The scale bar is given in arbitrary units of X-ray diffraction peak intensity. An X-ray diffraction pattern was collected every 20 minutes during a galvanostatic charge to 4.8 V and discharge to 2 V of ball milled $Li_2CuP_2O_7$ at a $C/10$ rate.

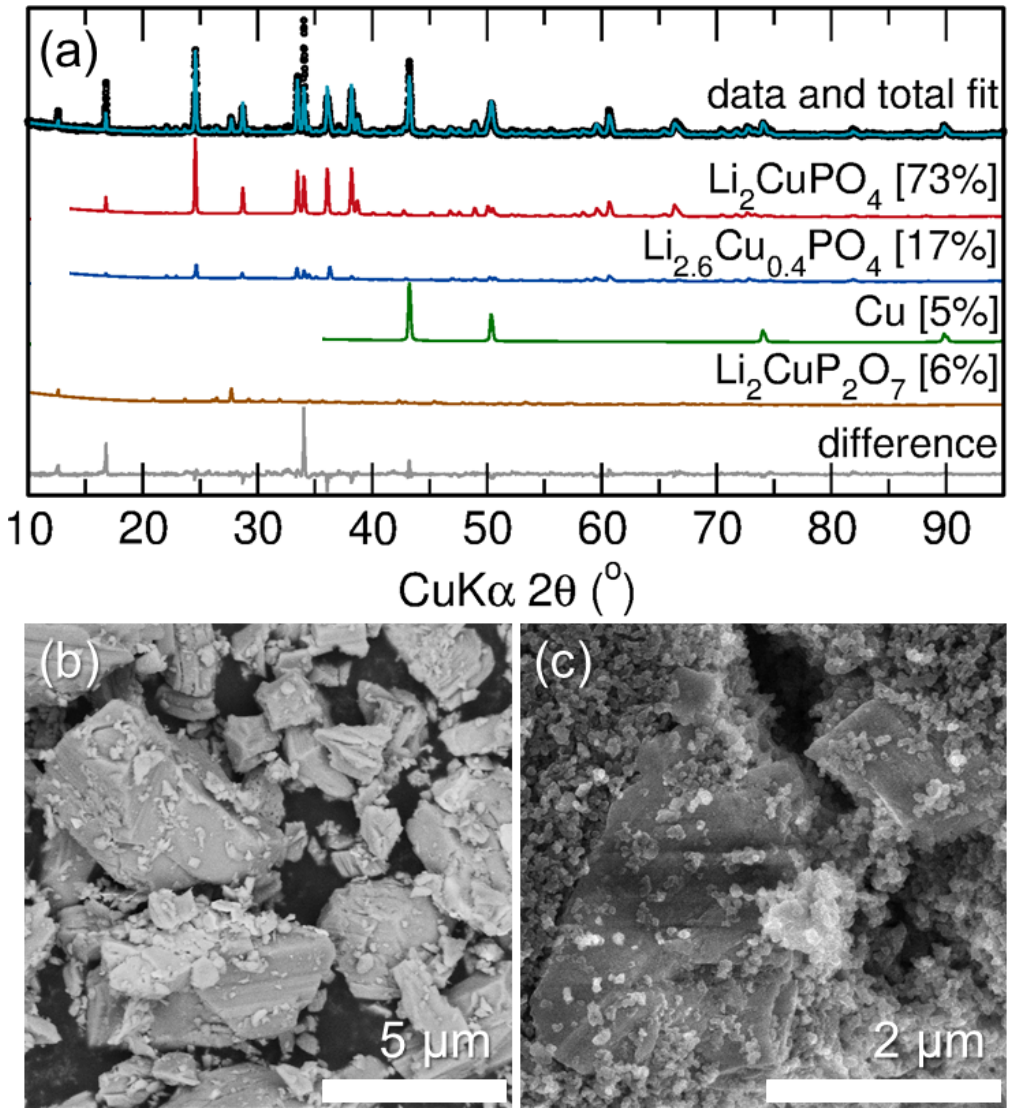

Figure S3: (a) Rietveld refinement of the powder X-ray diffraction pattern of the furnace prepared Li_2CuPO_4. (b) Scanning electron micrograph of furnace prepared Li_2CuPO_4 particles ranging in size from sub-micron to 5 μm in diameter, and (c) the same particles after ball milling with graphitic carbon prior to electrochemical testing - particles range in size from sub-micron to 2 μm in diameter.

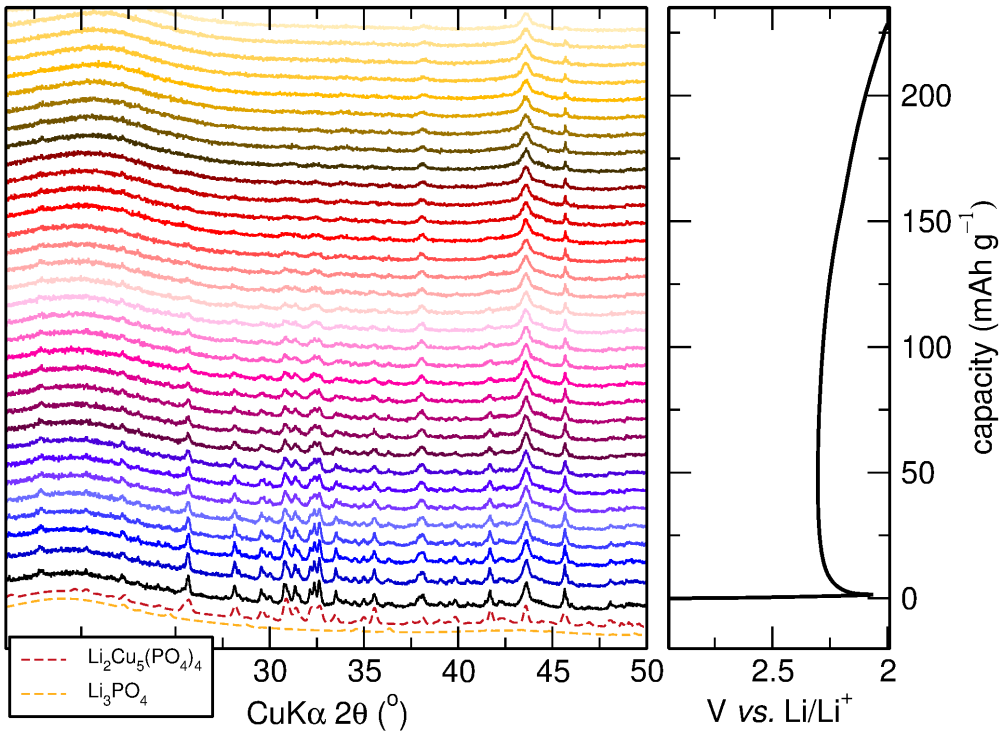

Figure S4: *Operando* X-ray diffraction measured every 20 min during a galvanostatic discharge to 2 V of ball milled $Li_2Cu_5(PO_4)_4$ at a $C/10$ rate. Below the incremental XRD scans, which peaks correspond to the $Li_2Cu_5(PO_4)_4$ active material and which peaks correspond to the Li_3PO_4 secondary phase are indicated.

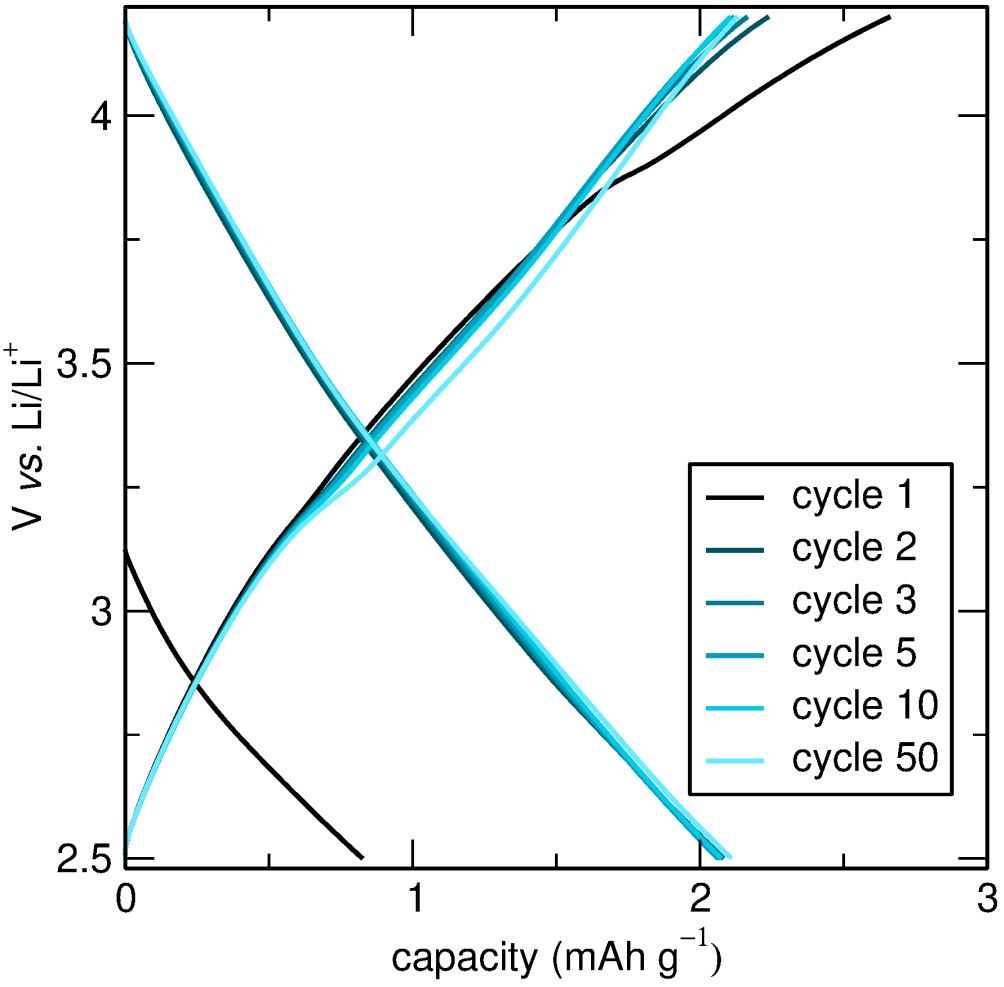

Figure S5: Galvanostatic cycling of ball milled $Li_2Cu_5(PO_4)_4$ at a $C/60$ rate between 2.5 V and 4.2 V. Essentially no capacity is demonstrated.

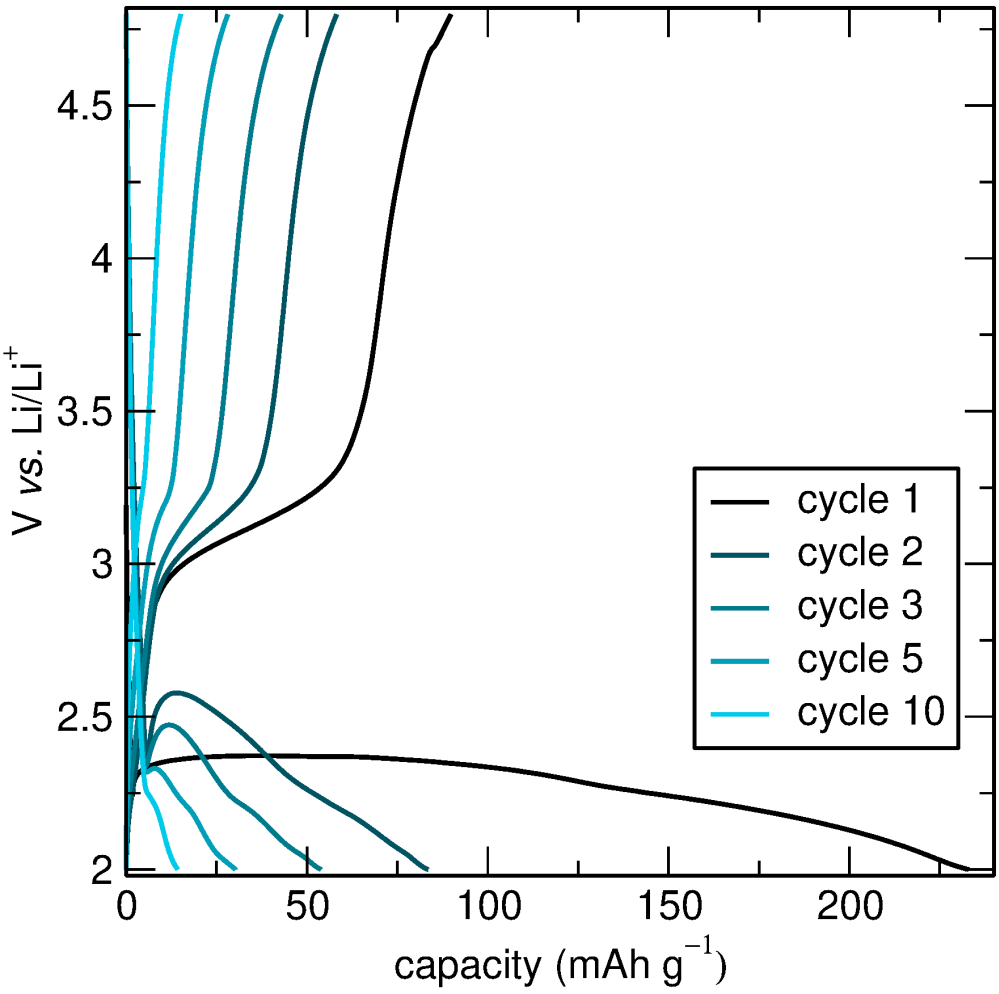

Figure S6: Galvanostatic cycling of ball milled $Li_2Cu_5(PO_4)_4$ at a $C/60$ rate between 2 V and 4.8 V.